

An "oriented-object" computer construction of deforming fractal soil structures. Determination of their water properties

E. Perrier, C. Mullon, M. Rieu and G. de Marsily

Abstract: In order to study relationships between soil water properties and soil structural properties, a computer micro-model of soil is constructed. In this paper, we present first a general building method of a porous structure, including both pores and grains, with different levels of aggregation resulting from a fragmentation process. A fractal structure is obtained when self-similarity is imposed over the successive scales of fragmentation.

Emphasis is put upon the modeling of the retention curve. A classical capillary model and methods coming from the percolation theory enable us to simulate qualitatively the primary and secondary loops of the well-known hysteresis of this curve. In the fractal case, theoretical analytical expressions proposed for adjusting retention data are tested.

The unsaturated hydraulic conductivity is also calculated on the same simulated soil, by analogy with an electrical network.

On the other hand, our structures are deformable and simulation proves to be a useful tool to investigate the behavior of swelling soils.

1. Introduction

The knowledge of the specific hydraulic behavior of a given soil is needed for the purpose of modeling water transport in the unsaturated zone. The soil water properties, mainly the retention and conductivity curves are usually determined under controlled flow experiments either in the laboratory or in the field. It is an old dream among soil scientists to relate directly these water properties to structural properties which could be obtained more easily on dry soil samples.

Numerous attempts have been made to find either statistical relationships or deterministic links between structural data and water properties. We are interested in this paper in the deterministic approach.

Research has been done (Arya&Paris 1981, Haverkamp&Parlange 1986, Tyler& Wheatcraft 1989/1992) to link water properties to the particle-size distribution of a soil, which is structural information that is easily and widely obtained through mechanical sieving. The texture models that define the soil from matrix properties such as grain diameter or grain shape (e.g the spheres models) view the solid phase as a set of discrete grains and the void phase as a continuum. The complex geometry of the remaining void space makes the analysis of flow too difficult unless one works at the Navier-Stokes scale (periodic grain patterns for analytical work or any pattern but only a few grains in lattice gas simulations). At the pore scale, we have to partition the pore space in a set of simple geometrical parts, such as cylinders or parallepipeds, in order to use integrated forms of fluids properties. So a common approach consists in inventing a pore space model with simple geometry that could be associated to the particle distribution. For example, Arya & Paris associated a tube to each particle-size class and treated the pore space as a bundle of capillary tubes. But in order to obtain good agreement between calculated and observed retention data, they needed to add an empirical fitting parameter. It's clear that water flows through the voids of the soil, and transport properties are induced by the pore geometry. So the point there is to find how a pore distribution can be related to a given particle distribution.

On the other hand, many authors based their modeling approach directly upon the pore distribution. The solid phase is viewed as a continuum, cut through by a set of discrete pores and its geometry is considered to be irrelevant to flow transport. Generalizing the bundle of tubes associated to distinct pore-size classes to a continuous pore distribution, Mualem (1974,1976) predicts retention and conductivity curves by integration of the pore-size distribution density function while others (Thirriot 1981/1982, Billotte 1986) deal with inter-connected tubes in a probabilistic manner. But use of computer has soon allowed to simulate the soil porosity by a network of tubes which represents more closely real porous media (Fatt, 1956) than the oversimplified bundle and takes account of the topology of the pore space. Thereafter, considerable work has been done on pore or fracture networks (Chatzis&Dullien 1982, Lenormand 1986, Charlaix 1987, Billaux 1990, Daian&Saliba 1991) within the general framework of the theory of percolation in disordered networks.

Anyway, if we want to use a network model on a real soil, we have to know which pore distribution to enter in the model. We can choose the distribution resulting from image analysis or mercury porosimetry measurements, that is mainly estimates of the pore distribution in a dry soil sample. But a lot of soils are more or less deformable: Even without any mechanical constraints, the grain packing changes with moisture state; the pore network evolves, while the particle distribution remains unchanged. Deformability is usually neglected in standard modeling. On the contrary, we believe that better knowledge of the structural organization of the soil can be deduced from precise deformability measurements. So the point here is to find how we can obtain reliable information about the effective pore size distribution.

2. Construction of soil structures.

Our approach is based on a new approach in computer science, where the concept of "simulated reality" is popular. We construct samples of soil structures in order to study their soil water properties. "Such simulations are based on the construction of microworlds where particular hypothesis can be explored, by controlling and repeating experiments in the similar way as real experiments are performed in a real laboratory." (Ferber&al, 1991)

We intend to build a complete porous structure which could take into account both solid and void phases at the microscopic scale: our construction will be a structured set of individual grains and pores; two main characteristics of the structure will be a particle-size distribution (*PSD*) and a pore size-distribution (*psd*).

We are particularly interested in the behavior of swelling soils where shrinking and swelling phenomena occur with variations in moisture content: we will define deformable convex areas representing aggregates of grains to manipulate isotropic deformations.

We work here in 2 dimensions; surfaces represent volumes and are extrapolated to 3 dimension by means of calculus when numerical results are needed.

2.1 Construction on one level of fragmentation. The sample of studied soil is represented by a polygonal area A_0 , generally a square. A fragmentation process is simulated: a set of initial points (fragmentation seeds) is generated inside A_0 . Then a space partition is realized to split A_0 into polygonal zones surrounding each point (Fig 1): the polygonal area P associated with a point M is the set of points whose nearest seed point is M (Fig 2a). The algorithm is named a "voronoi tessellation" and consists in a rather complicated determination of successive perpendicular bisectors between 2 points next to each other. We obtain an irregular grid which is the invariant skeleton of the structure (Fig 1 and Fig 2a).

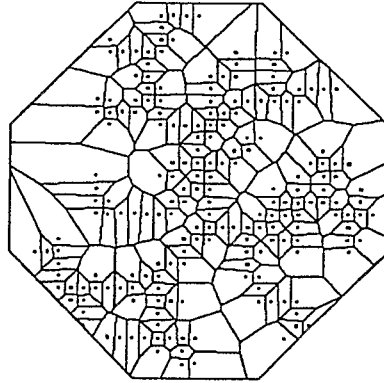


Fig1: A Voronoi tessellation with a specific set of initial points.

Any initial set of points is possible. The "random" case reported in this paper refers to a set of points generated with uniformly distributed co-ordinates.

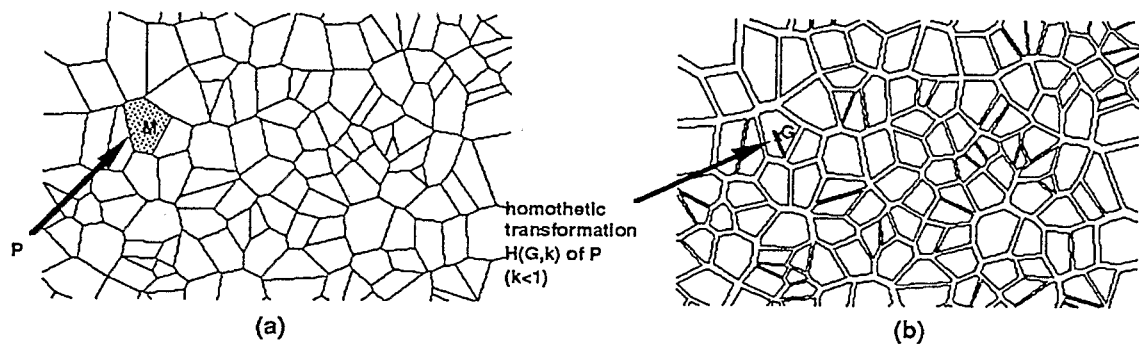


Fig2: A tessellation with a random initial set of points.
(a) Structure skeleton (b) Pores and grains.

Then we create a porous structure and a given porosity by means of an homothetic reduction $H(G,k)$ of each initiating zone P (Fig 2 b): k is a number less than 1 and G is the center of gravity of the convex polygon P (If P is located on the outer edge of A_0 , then G is displaced onto the outer face of P to avoid edge effects). The reduced polygon represents a grain; the opening between two grains represents a pore.

One component of the model is an irregular pore network which yields the geometrical constraints imposed by the space partition into either solid or void objects.

The particle and pore surfaces are calculated for each grain or particle and summed within any size class (Fig 3).

An undeformable porous structure is defined by a skeleton and a homothetic ratio k . With a same value k for each polygon P , the PSD is proportional to the initial distribution of the polygonal zones and is entirely determined by the choice of the initial points. One single psd is associated to the particle distribution .

We can also construct other distributions by choosing an individual homothetic ratio k_j for each polygon P_j in a statistical number distribution .

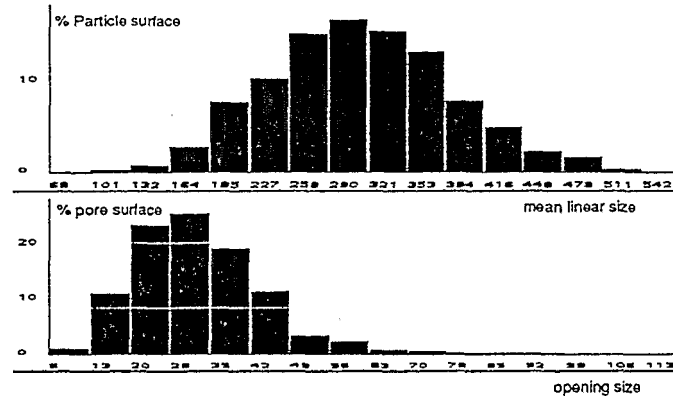


Fig 3: A single homothetic ratio k on a random structure: PSD and associated psd

2.2 Construction on several levels of fragmentation .

Real soils and particularly aggregated soils have often been described as porous media structured on different organization scales (Kutilek, present colloquium, 1992). For example, several authors (Van Genuchten, Gerke, present colloquium, 1992) work on soils presenting only "a dual porosity" on two levels.

The process described above can be repeated on successive levels of fragmentation. What we have called grains so far will represent now microporous aggregates that are divided into smaller aggregates. Once a set of points has been generated in the initial zone A_0 which fragmented into N_1 smaller zones A_1 , a new set of points is generated within each zone A_1 which determines a partition of A_1 into N_2 smaller zones A_2 and so on up to the ultimate level n of fragmentation . A new type of structure skeleton is obtained (Fig4a) Each zone A_i is divided into N_{i+1} zones A_{i+1} . Embedded aggregates of grains and pores are created in the same way: at each level i an homothetic transformation $H(G_i, k_i)$ is applied on the zone A_i with a given ratio k_i from the center of gravity G_i of A_i . The number N_i of sub-aggregates and the k_i reduction ratio can have any relevant values.

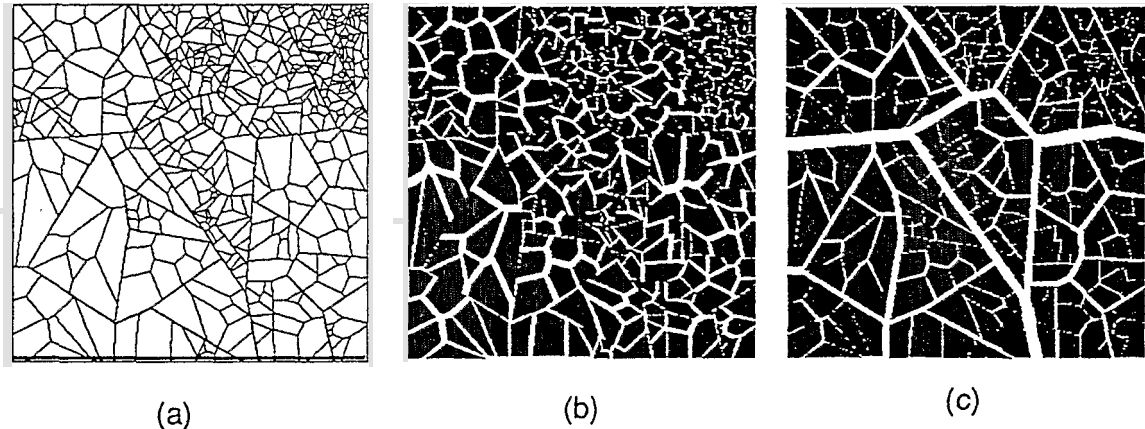


Fig 4: (a) Same structure skeleton. $n=3$. $N_1=N_2=N_3=N=8$.
 (b) Porous structure with $k_1=k_2=1, k_3=0.941$ ($k_0=1$)
 (c) Porous structure with $k_1=k_2=k_3=K=0.98$ ($k_0=1$)

A rigid porous structure is defined by a skeleton and a set $(k_1, k_2, \dots, k_i, \dots, k_n)$ of homothetic ratios, where the subscript i refers to the fragmentation level. However, intra-variability of k_i within any level i can be introduced.

Different models of soil structures corresponding to different types of aggregation in soils can be associated to the same PSD (Fig 4a and 4b). Different clustering patterns are simulated with the process of packing ($k_i < 1$) or non-packing ($k_i = 1$) into aggregates of level i and lead to different psd (Fig 5b and 5c).

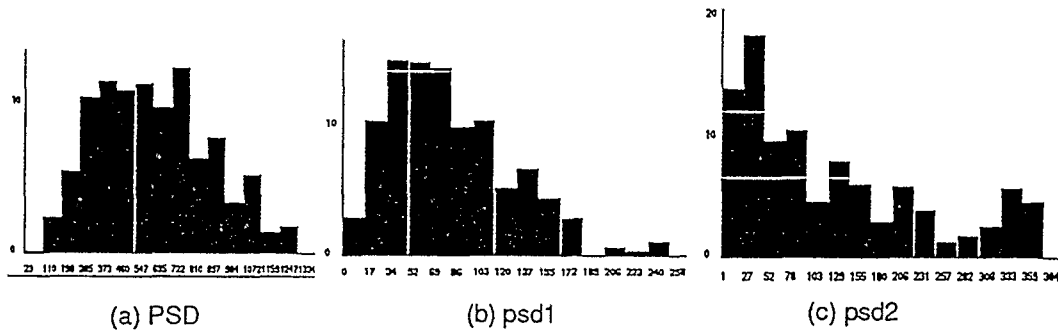


Fig 5: Same PSD and 2 possible associated psd1 (cf Fig 4.b) and psd2 (cf Fig 4.c)

2.3 Fractal structures. Fractal geometry has appeared to be a good tool for describing many porous media (Pfeifer&Avnir 1983, Degennes 1985, Katz&Thompson 1985, Jullien&Botet 1986, Friesen&Mikula 1987, Delannay&al 1989) and particularly soil structures (Tyler&Wheatcraft, 1989,1990,1992, Toledo&al 1990, Ahl&Niemeyer 1989/1991, Bartoli&al 1991, Young&Crawford 1991, Rieu&Sposito 1991). Rieu and Sposito described the observed similarity in the different organization levels of structured soils by means of a fractal model. In our construction, self-similarity can be produced (on average) by a constant number N of sub-aggregates "children" and the same homothetic ratio K for all the homothetic transformations on any aggregate at any level. The simulated porous structure is then a statistical realization of the theoretical fractal fragmented porous media proposed by these authors. According to the definition of the fractal dimension from self-similarity of a set of objects, the fractal dimension of the 3-dimensional soil corresponding to our simulated plane structure is $D = 3\text{Log}N/(\text{Log}N - 2\text{Log}K)$. Figure 4c shows an example where $D = 2.943$ ($N = 8, K = 0.98$).

2.4 Deformability This rather complex structure (see Appendix 1) has been imagined to enable the simulation of dynamic deformations. The figures 4.b and 4.c depicted two types of aggregation in different soils. They can also represent two stages of aggregation in the same soil at two distinct times t_1 and t_2 . For example, (b) could represent an opening state of a wet soil structure while (c) would represent the cracks after a drying process in a swelling soil. An opening state of a deformable porous structure at time t is defined by an invariant skeleton and a set $(k_i(t))_{i=0 \dots n}$ of variable homothetic ratios.

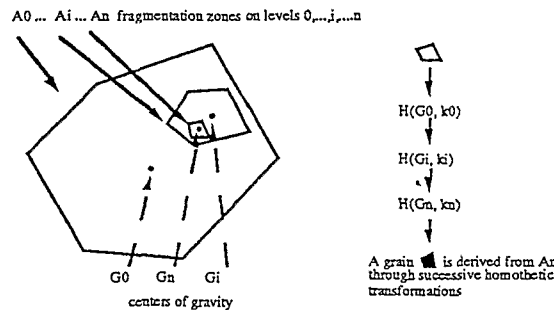


Fig 6: Fragmentation hierarchy and successive homothetic transformations

Let us recall that the skeleton occupies a total surface A_0 and is made of zones A_{ij} at each level of fragmentation i .

For a given opening state of the structure, the grain associated to any zone A_{nj} is a homothetic replicate of A_{nj} and its surface is $(k_0(t)k_1(t)\dots k_j(t)\dots k_n(t))^2 \text{surface}(A_{nj})$ (cf Fig 6). The only condition for realistic deformation is that the grains remained

unchanged, that is: $\Pi_n = \prod_{i=0}^n (k_i(t))^2$ must be independant of t .

Let us name S_i the total surface of aggregates of level i , S_n the total surface of the grains.

$$S_n = \sum_j \Pi_n \text{surface}(A_{nj}) = \Pi_n \sum_j \text{surface}(A_{nj}) = \Pi_n A_0.$$

In the same manner,

$$S_i = \prod_{j=0}^i (k_j(t))^2 A_0 = \Pi_i A_0,$$

and the total surface S_0 of the whole simulated sample is $(k_0(t))^2 A_0 = \Pi_0 A_0$.

S_0 (representing the measurable macrosocopic volume) can vary: the parameter k_0 was set to 1 for rigid structures; it can now take different values in swelling or shrinking soils.

S_n (representing the volume of the solid phase) must be constant.

S_i can have any value so long as aggregates don't overlap.

Hence, for the same PSD, multiple opening states of the structure can be simulated.

3. Simulation of the retention curve

3.1 Principle: A first component of the structure is a set of simple pores and the pore size distribution. The pores of our model are channels representing sections of 3-D fractures. We use a simple capillary model for interpreting the repartition of two non-miscible fluids in a porous media (the wetting fluid is here water while the non-wetting fluid is air), postulating Laplace's law to be valid throughout the whole pore distribution range in the following simplified manner:

for a given capillary pressure h and the corresponding equilibrium state,

A pore p is filled with water (resp air)

if its aperture is less than $r = \alpha / h$ (resp more than $r = \alpha / h$). (Condition 1)

where α is a constant which could be calculated from the liquid-solid contact angle and the liquid-vapor surface tension of water.

It is then easy to calculate a moisture content related to any pressure h by means of the pore distribution. At any given capillary pressure h , the water content is equal to the sum of the volumes of all the pores of aperture lower than r . The pore volume is calculated from pore surface as explained in Appendix 2. The capillary retention curve so obtained is named "reference curve".

A second component of the structure is a pore spatial distribution on a pore network.

The simulation of the invasion of a fluid in an interconnected pore network introduces a new idea: for the invading fluid to penetrate a pore, this pore must be reachable, that is connected to the supply faces. A connectivity condition is added:

A pore p may be filled with water (resp. air)

if it is connected to the supply face through a continuous path of water (resp. air) (Condition 2)

3.2 Description

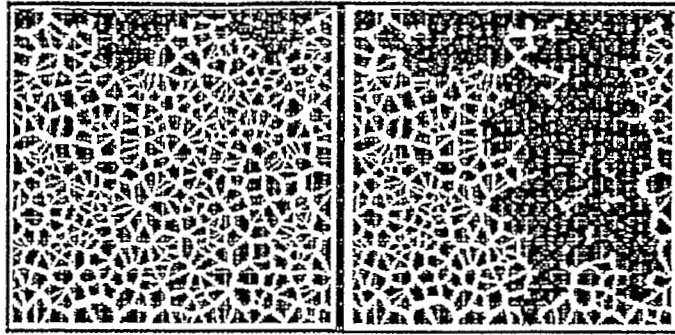


Fig 7: Invasion of water in a dry soil

For example, let us consider a square sample of entirely dry porous medium. Let us suppose that water is brought on the upper edge

We simulate successive pressure equilibrium states. For high pressure, water will first penetrate the narrowest pores but only those which are connected to the upper edge through a continuous supply path of water (Fig 7a). A capillary pressure decrease indicates that larger pores are filled with water, and the more pores are filled the more the invading fluid gains access to other pores (Fig 7b).

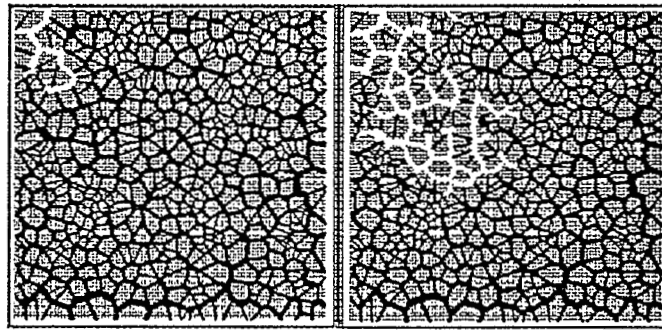


Fig 8: Invasion of air in a water-saturated soil .

The invasion of air in a medium initially saturated with water is simulated in the same way. Air flows first through the broadest pores, then through narrower pores with increasing pressure (Fig 8).

3.3 Simulation of the hysteresis of the retention curve.

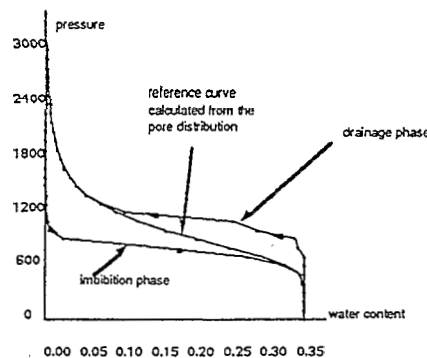


Fig 9: Hysteresis of the retention curve on a random structure

The connectivity condition yielded by the simulation of what is known as an "invasion percolation process on a network" (conditions 1 and 2) appears to be strong enough to result in the simulation of the well-known hysteresis of the capillary pressure versus water content relationship. The drainage and imbibition simulated curves are respectively located above and under the calculated reference curve as shown on figure 9.

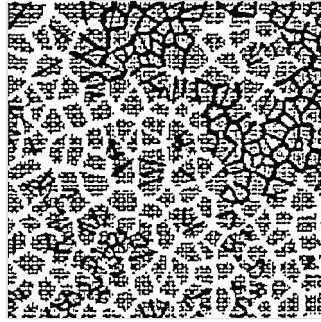


Fig 10: Invasion of water in a half-saturated medium.

If the simulation is applied to a variably saturated initial medium (Fig 10), the secondary hysteresis loops are reproduced too (Fig 11), in the same way. The connectivity condition 2 remains the same but its application requires an improved algorithm (a list of nodes must be used because usual progression of the invasion front from neighbors to neighbors no longer works)

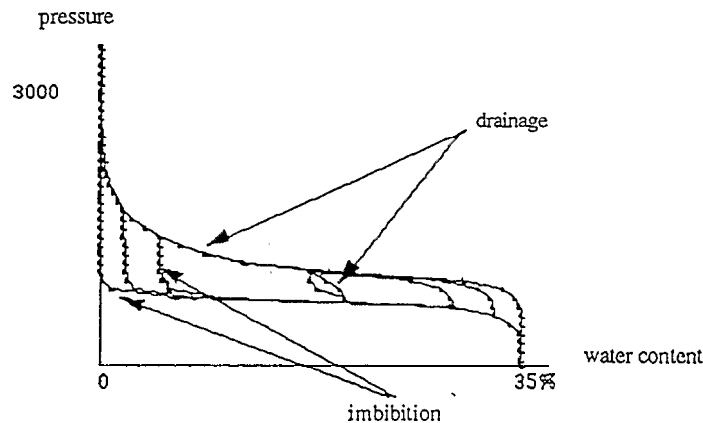


Fig 11: Simulation of the primary and secondary hysteresis loops.

The simulation principle reported here has often been used: different simulated drainage and imbibition curves have already been reported, but we are not aware neither of direct comparison between these two curves nor of the simulation of the secondary loops in the field of network modeling. Golden (1980) published a paper to show that the phenomenon of hysteresis (primary&secondary) can be derived mathematically from percolation theory applied on simple pore networks models. We check this qualitative theoretical result in any case. But, by actually simulating the shape of the loops, we obtain additional information. Later in the present paper, we will see special configurations where the loops join together and hysteresis disappears.

3.4 Simulation of the retention curve in fractal structures. The spatial repartition of the pores in the fractal construction implies that there is no problem of accessibility during the drainage phase. The hysteresis is mainly due to the imbibition curve (Fig 12).

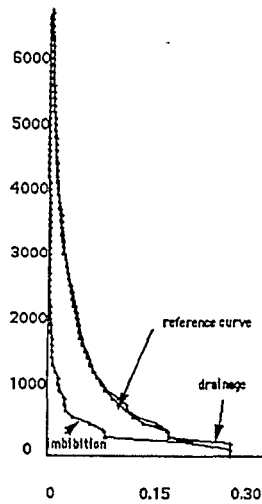


Fig 12: Retention curves in a fractal structure

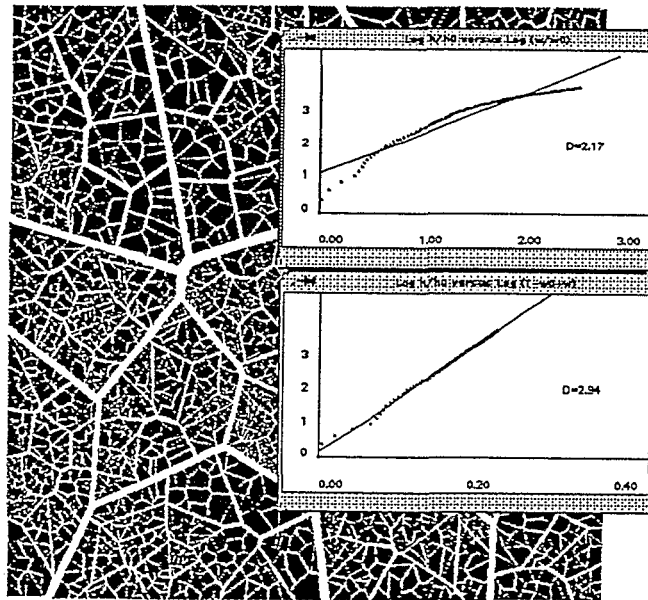
Let us build a fractal soil structure with a given fractal dimension D_{def} .

The simulation of successive equilibrium moisture states, produces simulated capillary drainage pressure data that fit quite well the theoretical analytical expression (1) proposed for modeling the pressure/water content (h, w) relationship in fragmented fractal soils (Rieu & Sposito 1991):

$$w(h) = (h/h_{min})^{D-3} + w_{sat} - 1 \quad (1)$$

(w water content, h capillary pressure)

On the other hand, the value of D derived from this adjustment is quite close to D_{def} , which confirms that we succeeded in the construction of a statistical realization of the theoretical perfect fractal model which was illustrated by cubic particles of single size.



$D_{def} = 2.95$. $D = 2.94$ ($R = 0.999/99pts$). $D' = 2.17$ ($R = 0.951/99pts$).

Fig 13: A fractal structure ($n=3, N=10, K=0.97$)
Log h / Log w plots of simulated data fitted to expressions (2) and (1)

The classic Brooks & Corey analytical expression (2) provides rather bad adjustments which suggest that this model may not be accurate for such fractal soils.

$$w(h)/w_{sat} = (h/h_{min})^\lambda \quad (2)$$

Other authors (Tyler & Wheatcraft 1990, Ahl & Niemeier 1991) propose a different fractal soil model and derive a fractal dimension D' from expression (2) with $D' = \lambda + 3$. We show that these two methods used for the determination of the fractal dimension from the retention curve are not equivalent at all (Fig 13) and lead to quite different fractal values on the same soil structure.

4. Simulation of Deformation.

4.1 Experimental data. An experimental device was developed by Braudeau (1988) to carry out on-line deformation measurements on drying structured soil cores. The device performs macroscopic linear measurements and deformation is assumed to be isotropic. A lot of characteristic shrinkage curves (Fig 14) relating the bulk core volume to the water content are easily obtained.

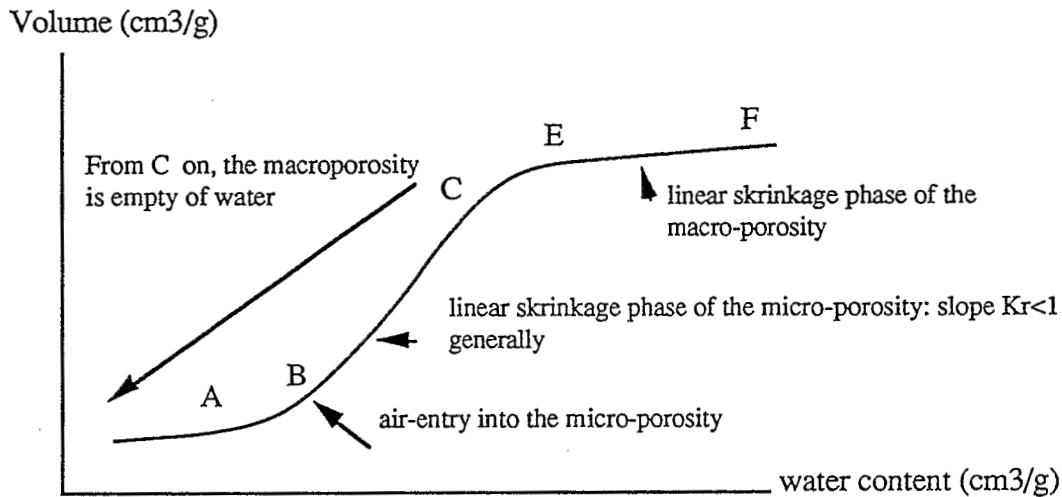


Fig 14: Typical experimental shrinkage curve of a ferrallitic soil and its main transition points interpreted by Braudeau's model

Different assumptions have been made to simulate the shrinking behavior of a soil. They are being tested to find what consequences they have on the soil water properties.

4.2 Principle. We again simulate successive equilibrium pressure states. But a variation in capillary pressure does not only imply a modification of the water content but also a possible variation in volume.

The simulation works in alternate phases of deformation then repartition of the fluids in the deformed structure. Each simulation step corresponds to a given pressure and is divided into two parts:

First phase of geometrical deformation of the structure:

If a condition for deformation have been fulfilled, the new opening state of the structure is calculated. Let us recall that an opening state of the structure is defined by a list of ratios $(k_0(t), k_1(t), \dots, k_i(t), \dots, k_n(t))$.

In this paragraph, the total surface S_i of aggregates of level i (cf 2.4) will be called volume V_i for reasons of better understanding but experimental data are linear

deformations that can be entered in 2-D simulations, assuming isotropy. If variations ($\Delta V_0, \dots, \Delta V_i, \dots, \Delta V_n$) are imposed on the open structure, the new state vector after deformation ($k_0(t+1), \dots, k_i(t+1), \dots, k'_n(t+1)$) is easily calculated from the state vector ($k_0(t), \dots, k_i(t), \dots, k_n(t)$) before deformation. The calculation is done from top level 0 to bottom level n in a recurrent manner.

The main assumption is that the filling state of the pores remains unchanged during the deformation phase.

Second simulation phase of re-equilibration of the filling state of the structure:

Then the filling or emptying of those pores which fulfill both conditions 1 and 2 is simulated as previously.

After each simulation step, graphics are redisplayed, and skrinking (or swelling) soils can be seen respiring while filling or emptying with water.

4.3 Simulations: The different scenarii of deformation consist in choosing ($\Delta V_0, \dots, \Delta V_i, \dots, \Delta V_n$) according to various assumptions and conditions. A variation ΔV_0 of V_0 expresses a measurable macrosocopic volume change. If the last stage of fragmentation n represents the grain scale as assumed until now $\Delta V_n=0$ (simulation 1). If n does not represent the actual last stage of fragmentation, but the last simulated stage, the aggregates of last level n represent microporous black boxes whose volume can vary (simulation 2). The following examples were simulated on the same skeleton ($n=3, N=10$) of the particular fractal structure shown on figure 13.

Simulation 1:

According to experimental data, a given law of macroscopic volume change related to total water content (Fig 14) is imposed. So ΔV_0 is known at each simulation step. And ΔV_n must be zero. On the other levels of aggregation any variation of volume can be chosen, so long as the particles do not overlap. In the case of figure 15, we assumed that $\Delta V_i = (1-i/n)\Delta V_0$.

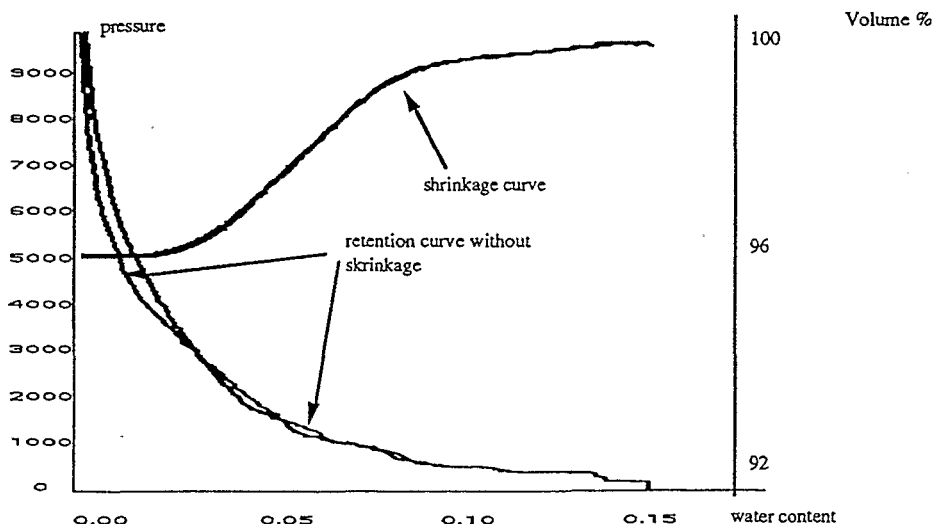


Fig 15: Simulation1:skrinkage curve imposed and compared retention curves

Simulation 2:

Braudeau(1988) proposed a model for interpreting shrinkage curves. He defines a dual porosity in soils, the intra-aggregates microporosity and the inter-aggregates macroporosity. From the point C to the end of the drying (Fig 14), the deformation would be entirely due to the microporosity of clayey aggregates whose elementary shrinking behavior follows that of pure clay (Fig 16): they shrink and remain saturated with water until the point B where air begins to enter them. To simulate this phenomenon, we achieve an incomplete fragmentation and the aggregates obtained on the last simulated level of fragmentation represent the clay aggregates.

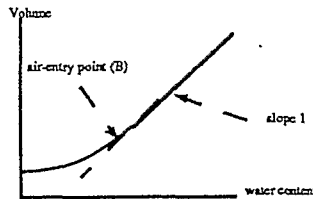


Fig 16: Shrinkage curve of a pure clay (Sposito, 1976)

We introduce their elementary behaviors in the simulation of the drainage of the macroporosity. Let us name w_{micro} the water content in the microporosity (into the black boxes) and add it to the simulated water content in the macroporosity. The drainage of the microporosity follows a theoretical law $h(w_{\text{micro}})$. On the last level n , $\Delta V_n = f(\Delta w_{\text{micro}})$ is according to figure 16. For the local deformations to be transmitted through the different scales of aggregation, one assumption may be: $\Delta V_i = K_r^{(n-i/n)} \Delta V_n$, where K_r is the main parameter of the experimental curve (Fig 14). Thus $\Delta V_0 = K_r \Delta V_n$ and K_r expresses the proportion of microscopic changes which are felt at the macroscopic level.

For the simulation to reproduce the part E-C of the shrinkage curve, where at the same time, the drainage of the macroporosity is simulated and the drainage of the microporosity is calculated, we assumed a quasi-linear $h(w_{\text{micro}})$ law.

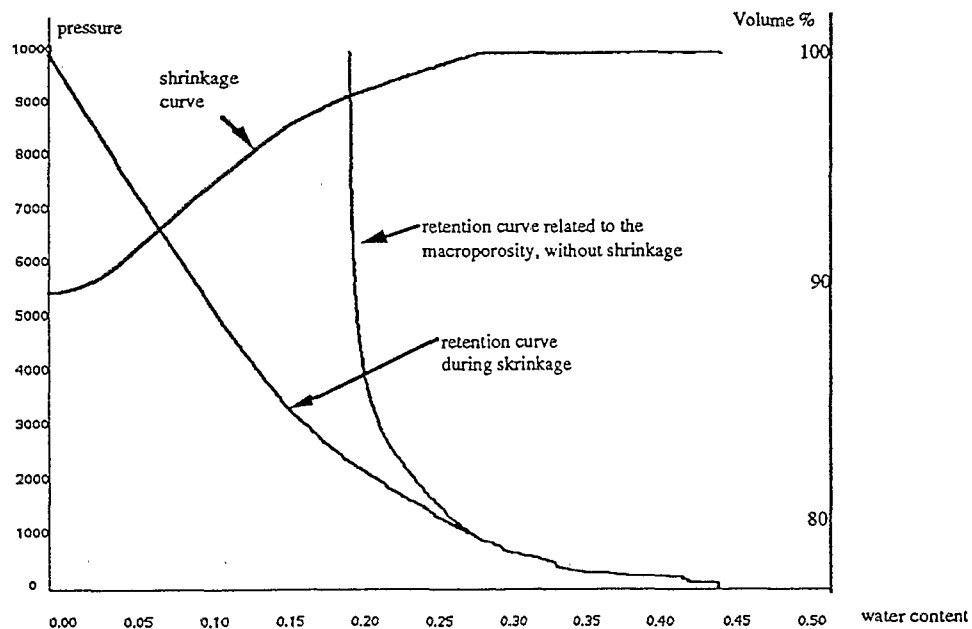


Fig 17: Simulation 2. Shrinkage curve and retention curve compared to the retention curve of the macroporosity without deformation

Boivin (1990) performed simultaneously retention measurements and shrinkage measurements. He showed that the data (obtained only during the first part of the drying process) did not fit the classical Van Genuchten model (1980) except if the pressure is plotted against the water content in the only macroporosity. The deformation simulated here modifies the retention curve in a similar way.

Whatever the assumptions are, the main result is a different psd between the wet and dry states. Simulation 1 leads to pores of reduced sizes in the dry soil, but the shape of those two psds are similar (Fig 19), because the deformation is uniformly distributed across the different levels of the structure.

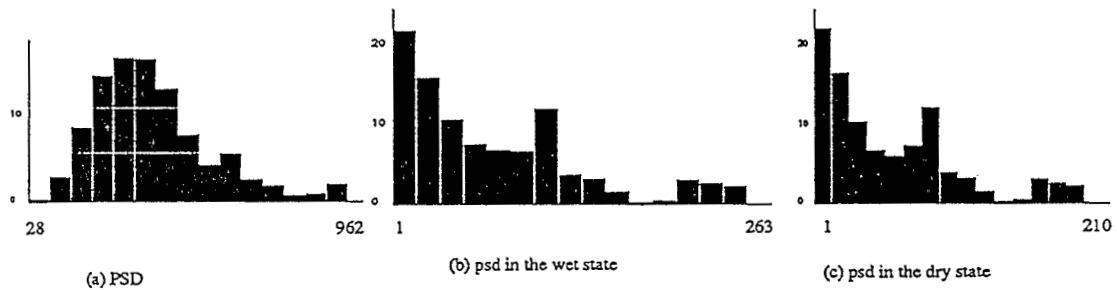


Fig 19: Simulation 1. Invariant PSD (a); psd before (b) and after (c) shrinkage

Simulation 2 exhibits only the modifications of the macro-pore system (Fig 20) whose volume increased because the micropores shrank more internally than the whole soil did. The PSDs of the figures 19a, 20a and 20b refer to the same skeleton: thus they have exactly the same shape.

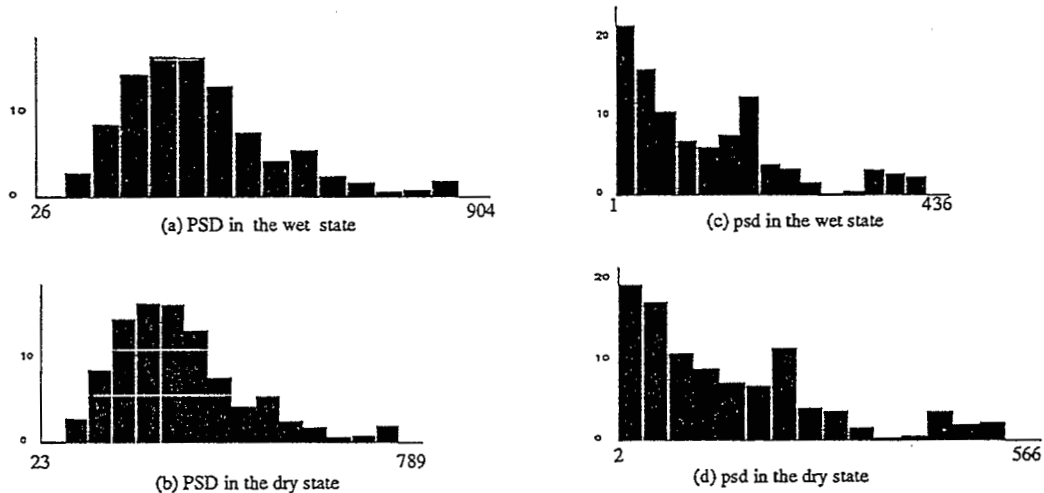


Fig 20: Simulation 2. Aggregate size distribution before (a) and after (b) shrinkage; psd before (a) and after (b) shrinkage

If experimental measurements were available, comparisons between dry and wet psds would allow to discriminate among the different possible assumptions made in the interpretation of the shrinkage process.

5 Simulation of the conductivity curve

5.1 Principle: The unsaturated hydraulic conductivity of the soil model is calculated by analogy with electrical transport. Each pore has an elementary hydraulic "resistance" varying as a power law of its aperture (In a fracture of aperture r and length l , the flow is proportionnal to r^3/l , according to the analog of Poiseuille law). At a given moisture content, if a pressure gradient is imposed between two opposite sides (Fig 21), water flows through the subnetwork of pores filled with water and connected both to the inlet and the outlet of the sample. The sum of the local flows at each internal node must be zero. This condition leads to a linear system to solve, imposing a precise potential at each point. The macroscopic equivalent resistance or hydraulic conductance is then derived.

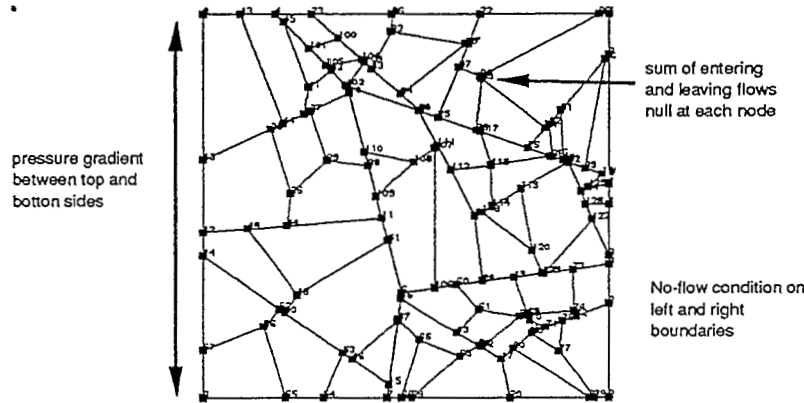


Fig 21: Method: Kirchoff network

5.2. First results: The results match a correct exponential shape above the "breakthrough" of water as shown on Figure 22.

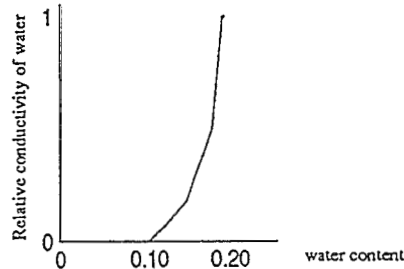


Fig 22: Simulated conductivity curve in imbibition on the soil structure of Figure 4.b

But, without any calculus, it is clear that this capillary conductivity is zero so long as no continuous path of water links the two opposite sides. Hence, on the random network, it is so under the percolation threshold for entering water, that is for low and medium water content. On the fractal structure, it is worse, because the belts of large pores surrounding the thin intra-aggregates pores prevent water from flowing except in saturated soils! Moreover, deformation emphasizes this problem with the formation of cracks in drying soils as shown on Figure 23.

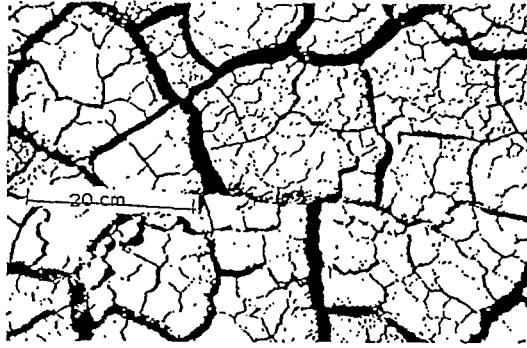


Fig 23: The surface of a vertic soil, drying (Photograph from North Senegal)

The problem is: How do micropores embedded into aggregates exchange water when the larger pores are empty?

5.3 Multiple plane realizations: Going on with a simple capillary model and neglecting diffusion in the vapor phase and thin films of water on the surface of the grains, we tried to improve the topological structure of our constructions. We supposed that some transversal connections and bridges between aggregates could exist in 3-D structures and performed several independant plane realizations linked by channels of variable aperture (Fig 24). A bijection is established from one node to its closer one in the following plane. Each node is connected to 3 neighbors in its own plane and to an other one in the next plane. In a two-planes realization, if two associated nodes are linked by an additional pore, 4 pores intersect in the same point ("coordinance" 4). If a virtual direct association is performed between two associated nodes, 6 pores intersect in the same place ("coordinance" 6). Multiple variants have been tested, which lead to analogs of square, or hexa-triangular networks while we delt with analogs to hexagonal networks in a single plane.

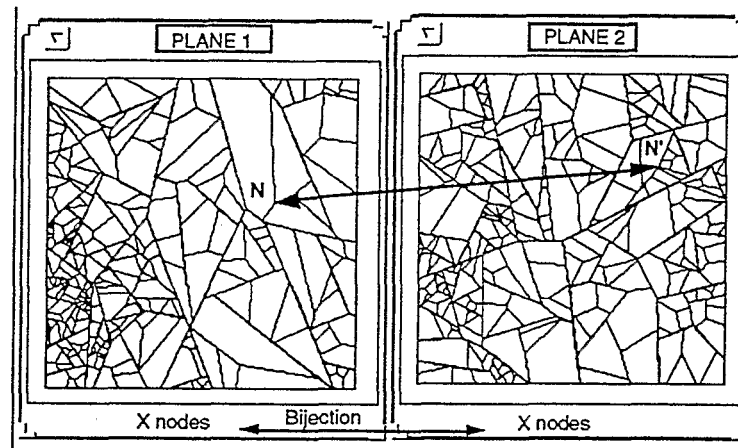


Fig 24: Bijection from node to node between 2 independant plane realizations.

A better connectivity is established and the shape of the conductivity curve is plausible (Fig 25).

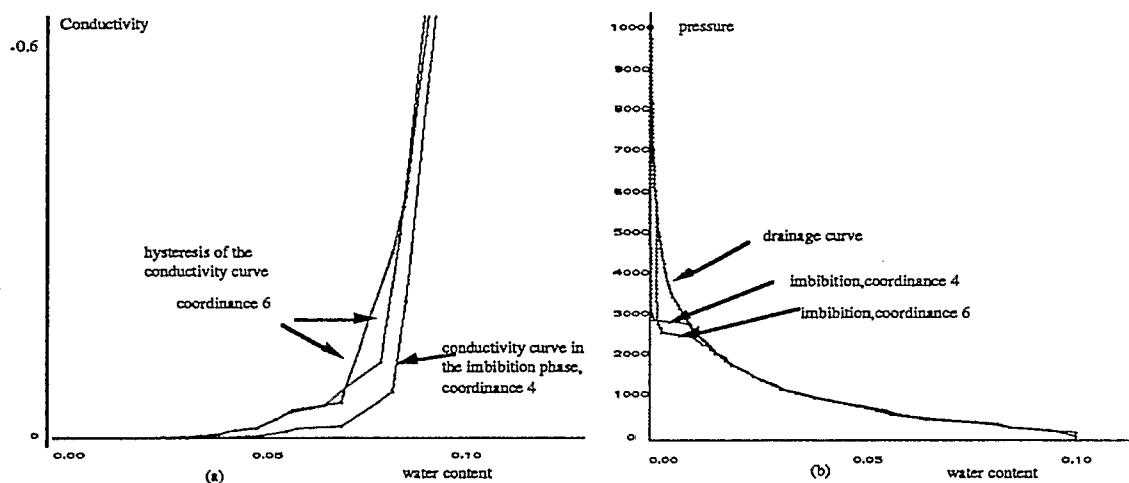


Fig 25: 2 planes. Result on a "fractal network"
 (a) Simulated hydraulic conductivity versus water content: a slight hysteresis
 (b) Almost no more hysteresis for the retention curve

But the more the coordinance of the pore network increases, the more the percolation threshold decreases, and when conductivity predictions are improved, the hysteresis of the pressure curve disappears. In the literature about classical random networks, we have not seen up to now conductivity curves and retention curves simulated on the same model both in drainage and imbibition and we do not yet know if our results can be generalized.

6. Conclusions

We show that the knowledge of the pore-size distribution is not enough to determine the water properties which are strongly dependent on the connectivity of the pore network. The spatial repartition of the pores which is linked to the particle aggregation state is the clue for both a good prediction of the hysteresis of the retention curve and an accurate prediction of conductivity. The fractal size distribution of the pore space may have been validated by the retention data in experimental studies, but the spatial repartition of this distribution remains an open question that must be clarified in order to predict realistic conductivity data. We are working at the moment on anisotropic fractal structures, where a modified aggregation process should allow for preferential flows of water at any water content while preserving the properties of the retention curve.

In this paper only construction algorithms and simulation principles are presented. On our simulated soil micro-model, we can easily "measure" at the same moment the main parameters of the structure and theoretical water properties. The results must be coherent or the model must be improved.

The choice of various initial distributions of particles, and the multiple ways to aggregate them can represent a large range of real soils. It is now possible to take into account the deformability that can bring new informations on the soil structure. These numerous possibilities have not yet been fully explored.

We aimed at developing an interactive and comprehensive computer tool for manipulating concepts on a simulated soil, and for testing previous theoretical models as well as new ideas.

REFERENCES

- Ahl C., J. Niemeyer, 1989. The fractal dimension of the pore volume inside soils. *Zeitschrift für Pflanzenernährung und Bodenkunde*.
- Ahl C., J. Niemeyer, 1991. Fractal geometric objects in the soil. AFRC engineering.
- Arya, L.M., J.F.Paris, 1981. A physicoempirical model to predict the soil moisture characteristic from particle-size distribution and bulk density data. *Soil Sci. Soc.Am. J.* 45:1023-1030.
- Arya, L.M., J.F.Paris, 1982. Reply to "comments on a physicoempirical model to predict the soil moisture characteristic from particle-size distribution and bulk density data". *Soil Sci. Soc.Am. J.* 46: 1348-1349.
- Bartoli F, Philippy R., Doirisse M., Niquet S., Dubuit M., 1991. Silty and sandy soil structure and self-similarity: the fractal approach. *J. of soil Science*, 42, 167-185.
- Billotte J.,1986. Modélisation de milieux poreux pour la détermination des paramètres nécessaires au calcul d'écoulements alternés. Thèse Ecole des Mines Paris.
- Boivin P. 1990, Caractérisation physique des sols sulfatés acides de la vallée de Katoure (Basse Casamance) Thèse Paris 6, Pédologie.
- Braudeau E.1988,Equation généralisée des courbes de retrait d'échantillons de sols structurés, C.R.Acad.Sci.Paris, t.307, Série II,1731-1734.
- Braudeau E.1988,Essai de caractérisation quantitative de l'état structural d'un sol basé sur l'étude de la courbe de retrait, C.R.Acad.Sci.Paris, t.307, Série II, 1933-1936.
- Braudeau E., 1988. Méthode de caractérisation pédo-hydrrique des sols basée sur l'analyse de la courbe de retrait. *Cah. ORSTOM, sér. Pédol.*,vol ,no 3: 179-189.
- Braudeau E., Boivin P., 1991. Transient determination of shrinkage curve for undisturbed soil samples: a standardized experimental method (à paraître Nato Asi Series)
- Charlaix E. 1987, Dispersion en milieu poreux: Mise en évidence de longueurs caractéristiques, Thèse Paris 6.
- Chatzis I., Dullien F, 1977. Modelling pore structure by 2-D and 3-D networks with application to sandstones *The journal of Canadian Petroleum*,
- Chatzis I., Dullien F, 1982. Mise en oeuvre de la théorie de la percolation pour modéliser le drainage des milieux poreux et la perméabilité relative au liquide non mouillant injecté. *Revue de l'institut français du pétrole*, Vol.37, n°2,183-205.
- Daian J.F, Saliba J. 1991. Détermination d'un réseau aléatoire de pores pour modéliser la sorption et la migration d'humidité dans un mortier de ciment. *Int. J. Heat Mass Transfer*. Vol 34, no 8,2081-2096.
- De Gennes P.G. 1985, Partial filling of a fractal structure by a wetting fluid. in "Physics of disordered materials, Adler & al, Ed. Plenum New York",pp 227-241.
- Delannay R., J.F.Thovert,P.M. Adler. 1989. Fractals et milieux poreux. *Revue internationale de systémique*, Vol.3,n°4.
- Drogoul A, J.Ferber, C.Cambier,1992, Multi-agent simulation as a tool for analysing emergent processes in societies, *Simulating societies symposium proceedings*.
- Fatt I,1956. The network model of porous media. I,II,III, *Transactions AIME*,vol 207,144-177.
- Friesen W.I, R.J. Mikula. 1987. Fractal dimensions of coal particles. *Journal of colloid and interface science*, 120: 263-271.
- Golden J.M. 1980. Percolation theory and models of unsaturated porous media, *Water Resources Research*, vol 16, pp 201-209.
- Guyon E., C.D. Mitescu,J .P Hulin, S. roux, 1989. Fractals and percolation in porous media and flows. PACS.
- Haverkamp, R.,J.Y.Parlange, 1982. Comments on a physicoempirical model to predict the soil moisture characteristic from particle-size distribution and bulk density data. *Soil Sci. Soc.Am. J.* 46: 1348.
- Haverkamp, R.,J.Y.Parlange, 1986. Predicting the water retention curve from particle-size distribution: sandy soils without organic matter. *Soil Sci.* 142:325-399.
- Jullien R., Botet R.,1986, Aggregation and fractal aggregates , Ed. World scientific.
- Katz A.J, A.H.Thompson, 1985. Fractal sandstones pores: implication for conductivity and pore formation. *Physical Review letters*, vol 54, no 12,1325-1328.
- Lenormand R.,1981. Déplacements polyphasiques en milieu poreux sous l'influence des forces capillaires. Etude expérimentale et modélisation de type percolation.Thèse ,Toulouse
- Mualem Y, 1974. A conceptual model of hysteresis. *Water Resources -Research*, vol 10 no 3:514-520.
- Mualem Y, 1976. Hysteretical models for prediction of the hydraulic conductivity of unsaturated porous media. *Water Resources -Research*, vol 12 no 6 :1248-1254.
- Pfeifer P., D. Avnir. 1983.*J.Chem. Phys.* vol 79. 3558.
- Rieu M., G. Sposito, 1991. Fractal fragmentation, soil porosity, and soil water properties: I Theory. *Soil Sci. Soc.Am. J.* 55:1231-1238
- Rieu M., G. Sposito, 1991. Fractal fragmentation, soil porosity, and soil water properties: II Applications. *Soil Sci. Soc.Am. J.* 55:1239-1244

- Sposito, G. et Giraldez J.V., 1976. Thermodynamic stability and the law of corresponding states in swelling soils. *Soil.Sci.Soc.Am.J.*,40 : 352-358.
- Thirriot C., 1981. Déplacement capillaire de fluides non miscibles dans un réseau de forme hexagonale. *C.R.Acad.Sc.* t.293:873-876.
- Thirriot C., 1982. Rusticité ou sophistication des modèles capillaires pour l'explication de l'hystérésis en milieu poreux. *Bull. GFHN.* no 11: 57-81.
- Toledo P.G, R.A Novy, H.T.Davis, L.E.Scriven, 1990. Hydraulic conductivity of porous media at low water content. *Soil Sci. Soc.Am. J.* 54: 673-679.
- Tyler.S.W, S.W. Wheatcraft ,1989. Application of fractal mathematics to soil water retention estimation. *Soil Sci. Soc.Am. J.* 53: 987-996.
- Tyler.S.W, S.W. Wheatcraft ,1990.Fractal processes in soil water retention. *Water Resources Research*, vol 26. pp 1047-1054
- Tyler.S.W, S.W. Wheatcraft ,1992. Fractal scaling of soil particle-size distributions: analysis and limitations. *Soil Sci. Soc.Am. J.* 56: 362-369.
- Young I.M, J.W. Crawford, 1991. The fractal structure of soil aggregates: its measurement and interpretation. *J. of soil Science.* 42:187-192.
- Van Genuchten M.T,1980. A closed form equation for predicting the hydraulic conductivity of unsaturated soils. *Soil Sci. Soc.Am. J.* 44:892-898.

APPENDIX 1: An insight into the computational "oriented-object" construction:

First of all, let us mention that the programs are written in C++ (oriented-objet version of the C programming language), use an Xwindow environment (oriented-object windowing system), and are implemented on a Sun Workstation. The program manipulates numerous computational entities (instanciated from some generic classes) which record in the same location of computer memory their own definition, the knowledge of their spatial or relational environment and their own behavior when local or global variations occur in the system. The maximum of information is encapsulated into the objects themselves to make the main program manage more easily complex situations.

The "oriented-object" modeling doesn't treat globally the reality but parts it into elementary functional components and is made easier by the use of appropriate programming languages.

class definitions

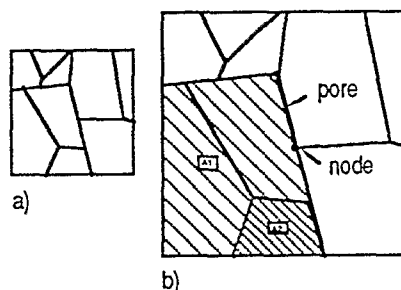


Fig 1: a) structure skeleton (n=2 levels, N=3 sub-aggregates at each level)
b) objects manipulated by the program

The main objects of the construction are aggregates, pores, and nodes. Classes of objects are computational declarations where definitions as well as properties of these objects are recorded.

An aggregate is defined as:

- a polygonal zone defined by the partitioning process at any level of fragmentation.
- an integer recording the level of fragmentation
- pointers indicating which the parent aggregate is in the fragmentation hierarchy.
- pointers referring to the neighboring aggregates within the parent
- an homothetic ratio
- deformation methods

A node is defined as:

- a point at the cross-section of lines in the structure skeleton
- pointers referring to the neighboring nodes

A pore is defined as:

- the segment defined by two neighboring nodes.
- pointers towards all the aggregates zones whose reduction creates part of the total opening of the pore
- method for calculating aperture and volume for each structure opening state
- methods for modifying its water content

Structure creation

All these objects are created with dynamic allocation of the computer memory (16 M in our case) to allow for various configurations

The structure skeleton is the main part of the construction

The aggregates are created with the tessellation algorithm already mentioned and their neighbors within aggregates' parent are recorded at the same moment.

The nodes are the polygon vertices and a rather complicated algorithm looks for node neighbors across the successive levels (3 neighbors in the general case).

The porous medium is the result of the simulation of a given "opening state" of the structure skeleton ;It is defined by a list of homothetic ratios (k_0, k_1, \dots, k_n). Its geometry is represented on the following figure. The surface of a pore is the sum of the surfaces of the trapeziums resulting from the different homothetic transformations and from the exact space partition. Each pore has a constant aperture over the main part of its length.

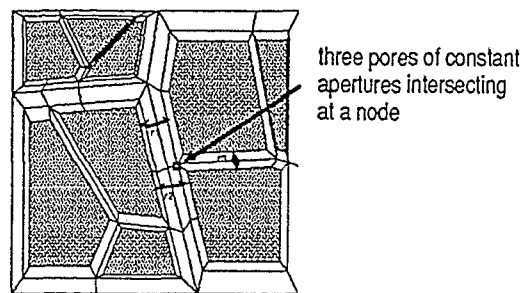


Fig 2: Pore geometry

Once the underlying program structure has been forgotten, the figures will only show an opening state of the structure as follows.

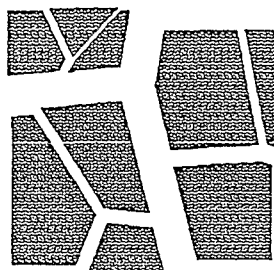


Fig 3: An opening state of the structure skeleton of figure 1

APPENDIX 2

How do we calculate the water content of any pore? We know the surface $S\%(p)$ of a pore p (expressed in percentage of the total simulated surface of soil); the corresponding volumetric water content $V\%(p)$ of this pore is equal to $S\%(p)$ if the fractures have an infinite extension in the third dimension, which isn't simulated. But if we suppose that the fragmentation process is isotropic, the volumetric porosity is higher than the surfacic porosity. We have chosen the formula

$$V\%(p) = 3/2 S\%(p) - 1/2 (S\%(p))^2$$

where $1/2 S\%(p)$ represents the percentage of porosity in each space direction and $1/2 S\%(p) * S\%(p)$ represents the intersections that must not be taken into account twice.

We work on representative sections of the porous soil. On random sections of a 3-D objet, another formula would have been $V\%(p) = S\%(p)^{2/3}$. The results obtained with these two expressions are close to each other.

Addresses of the authors:

E. Perrier, Laboratoire d'informatique appliquée / Laboratoire d'Hydrophysique ORSTOM. 70,74 route d'Aulnay. 93140. Bondy Cedex. France.

C. Mullon, Laboratoire d'informatique appliquée ORSTOM. Bondy. France.

M. Rieu, Laboratoire d'hydrophysique. ORSTOM. Bondy. France.

G.de Marsily, Laboratoire de géologie appliquée, UNIVERSITE Pierre et Marie Curie, 4, place Jussieu. 75252. Paris Cedex 05. France.



Scientific colloquium

*Porous or fractured unsaturated media:
transports and behaviour*

E. PERRIER, C. MULLON, M. RIEU, G. de MARSILY

October 5 - 9 / 1992

Monte Verità, Centro Stefano Franscini - ETH - Zürich
Ascona, Switzerland

Organized by :

SWISS FEDERAL INSTITUTE OF TECHNOLOGY OF LAUSANNE (EPFL)

- Land and Water Use Institute (IATE)
- Soil, Rock and Foundations Institute (ISRF)

UNIVERSITY OF NEUCHÂTEL

- Center of Hydrogeology (CHYN)

ORSTOM Fonds Documentaire.

N° : 41.30541

Cote : B